A Preliminary Study of Laser Directional Solidification for Potential Use in the Repair of Damaged Aviation Turbine Blades

Aiyong   CUI *, Haodong   LIU, Changliang   LU, Huakai   WEI, Bin   HU

Naval Aeronautical University, Qingdao Campus, Siliu Middle Road, Licang District, Qingdao, Shandong, China, 266041

To achieve directional solidification repair of damaged aviation turbine blades, the directional growth repair layer was prepared using a Nd:YAG laser on the surface of superalloy DZ-22. A scanning electron microscope (SEM) was used to observe the microstructure. The element distribution was analyzed and the microhardness of the sample was measured. The results showed that primary dendrite size was proportional to the current and the pulse-width, and inversely proportional to the scanning speed. No obvious macrosegregation of the repair zone was evident. The zone exhibited a finer microstructure than the substrate and had a smaller columnar crystal size, which was approximately two orders of magnitude smaller than the substrate. The micro-segregation between the centers and the edges of the dendrites and in between adjacent dendrites and a decrease in microhardness from the repair zone (455 HV) to the substrate also were observed.

Keywords: laser directional solidification, aviation turbine blade, microstructure, micro-segregation, cracking.

1. INTRODUCTION[*]

The repair and secondary use of damaged turbine blades has become a hot topic in the aviation field, with the increasing use of directional solidification techniques and single crystal superalloys in the blades [1]. For the repair of turbine blade damage by directional solidification, it is necessary to ensure that the crystallization direction of the new casting part is consistent with the original direction. Otherwise, even if the repaired zone appears to be integrated with the original blade, it will fail by peeling off from the substrate under the action of high temperature and heavy loads [2].

At present, the commonly used directional solidification technology includes Bridgman directional solidification, the electron beam directional solidification, light suspension directional solidification, whole directional solidification, electromagnetic cold crucible directional solidification and so on. However, directional solidification casting produces coarse crystal grains and severe segregation of alloying elements. Such components are difficult to repair by traditional techniques, and the heat input required is large. The heat-affected zone is prone to hot cracks. In addition, the high heat input causes the blade to re-melt and recrystallize locally, destroying its directional characteristics and affecting the service life [3 – 7].

For the preparation of aero-engine blades with complex sections, the difficulty in obtaining continuous directional solidification is to maintain a constant high temperature gradient in front of the solidification boundary. However, this depends not only on the ambient temperature gradient, but also on the cross-sectional area of the blade. The change of section area will change the latent heat release of the front edge of solidification interface. And then, local temperature gradient is affected, growth balance is destroyed, and heterocrystals are formed. Therefore, the development of new directional solidification technology is the trend of reparing aero turbine blades [8].

Laser directional solidification is a method that takes advantage of the steep temperature gradient and rapid solidification rate of the laser to create directional grain growth in the material within the molten pool. Local heat and low heat input. The direction of growth aligns with the orientation of the substrate and hence realizes the repair of the blade. Jianwei Liu [9], Wei Shang [10] simulated the crystal grain structure of aero-directional solidified blades and predicted the grain divergent growth under a specific process, but did not conduct experimental verification. Baocai Sun [11], Haibo Tang [12], Dongyun Zhang [13] studied the effect of laser directional solidification process on the structures of DZ125 alloy blades, Rene80, nickel-based superalloy and so on. But few studies were reported on laser directional solidification repair of damaged aeronautical DZ22 turbine blades, which is widespread applied. So, with the advantages of local heat generation, low heat input and ultrahigh temperature gradient, the laser repair approach is of great engineering significance to study the directional growth and the effectiveness of repair technology of turbine blades.

2. METHODOLOGY

2.1. Materials

The experimental material used was the aeronautical DZ22 substrate with a thickness of 5 mm, which was purchased and annealed from Western Titanium Technologies co., LTD (Shaanxi, China). The chemical composition is shown in Table 1. The chemical

---

[*] Corresponding author. Tel.: 13285326895.
E-mail address: *caylaser@163.com* (A.Y. Cui)

composition of the homemade alloy powder is shown in Table 2. The powder has a purity of 99.9 % and a particle diameter of 20 μm ~ 40 μm and was fully mechanically mixed after grinding and prepared by the coaxial powder feeding method.

2.2. Experimental procedure

A JHM-1GX-200B pulsed Nd:YAG laser was used for the experiment, and the robot (Japanese ERCR-HP3-AA00) was used as the actuator. The process parameters are as following: single pulse energy of 100 J – 150 J, scanning speed of 3 mm/s – 6 mm/s, pulse width of 8 ms – 15 ms, frequency of 6 Hz – 12 Hz, and light spot diameter of 2.5 mm. The process was protected using high purity argon. The overlapping ratio of multi-pass layers is 30 %.

2.3. Performance test

The morphological and structural characterizations were performed using a Toyota Hitachi S-3500N scanning electron microscope (SEM). The chemical composition of the samples was studied by X-Ray energy dispersive spectroscopy (EDS, INCA, Oxford, UK). The evolution of corrosion was measured by the TG-328A photoelectric analytical balance. The microhardness was measureed by a HXS-1000AK electronic microhardness tester (load 500 N, time 20 s).

3. RESULTS

3.1. Microstructure analysis

The microstructure of the repair zone for different laser pulse energy, as observed by SEM, is shown in Fig. 1. When the energy was set to 100 J (density 1415.4 J/cm^2), the direction of the columnar crystals of the upper middle section of the repair zone was not uniform. There were non-zero angles between adjacent dendrites. There was a shift in the direction of the dendritic growth and dendrite growth was discontinuous. When the energy reached 110 J, the direction of dendrite growth tended to be uniform and a few secondary dendrites began to appear. The spacing between the primary dendrites was larger than that in the bottom part of the weld. The thickness of the dendrites also increased. These observations, which were in agreement with the conclusions reported by Kurz et al [14], arose from the fact that the middle part of the repair zone had a smaller temperature gradient and a larger solidification rate than did the bottom part of the repair zone. The thickness and the spacing of the primary dendrites, as well as the number of secondary dendrites, keep increasing when the energy was set to 120 J (density

1556.9 J/cm^2). The columnar crystals on the top of the repair zone started to become isometric. When the current was increased to 130 J, growth of the columnar crystal was clearly observed. Primary dendrites became thinner while the secondary arms grew rapidly and were aligned well with the primary dendrites. The primary dendrite spacing continued to increase when the current was set at 140 J, as did the number and the size of the secondary dendrites. When the current was as large as 150 J, the columnar grains on the top of the repair zone started to disappear and small isometric crystals were formed instead, which were closely aligned. As the height of the repair zone was increased, the isometric crystals start to become disordered.

SEM images of the repair zone under different laser pulse-widths are presented in Fig. 2. It can be observed that under small pulse-widths the columnar crystals grew significantly (Fig. 2 a – d). With greater pulse-width, more of the secondary dendrites were evident and the primary dendrites became thinner. Under large pulse-widths (Fig. 2 e – f), both columnar crystals and equiaxed crystals were present. Secondary dendritic growth was boosted, while the columnar crystals started to change into equiaxed crystals. The pulse-width parameter affected the repair zone structure in a similar way to the pulse energy: it modifies the temperature gradient and solidification speed of various parts in the molten pool by controlling the heat input to the pool, and hence it governs the transition between columnar crystals and equiaxed crystals. Thus, it could be concluded that within the laser parameter range, small pulse energy and low pulse-width is beneficial to increase the columnar structure and suppress the growth of secondary dendrites.

SEM micrographs of the cladding layer with different scanning speeds are shown in Fig. 3. Compared to high-speed scanning, low-speed scanning provides a larger columnar crystal area in the repair zone. When the other parameters are fixed, a higher scan speed was less favorable for the formation of the columnar crystals. With increasing scanning speed, the directionality of the growth of the dendrites is progressively worse. Also, the transverse temperature gradient effect is more significant, and the preferred growth direction of dendrites is affected.

Zhang [13] discovered that the primary dendrite size is positively and negatively correlated with the laser power and the scanning speed, respectively. This is consistent with observations during the present study. Additionally, at high scanning speed, it is difficult to observe a through-going columnar structure in the repair zone.

Table 1. Chemical compositions of DZ-22 (wt.%)

C	Mn	Si	S	P	Ni	Cr	Al	Ti	Hf	Co	W	Nb
0.15	0.15	0.1	0.01	0.008	59.78	8.8	5.0	2.1	1.6	9.5	11.8	1.0

Table 2. Chemical compositions of in-house alloy powder (wt.%)

Cr	Co	W	Ti	Mo	Al	Fe	C	Ni
18	15	1.5	5	3	2.5	0.5	0.1	54.4

a – 100 J (1415.4 J/cm^2)

b – 110 J (1556.9 J/cm^2)

c – 120 J (1698.5 J/cm^2)

d – 30 J (1840 J/cm^2)

e – 140 J (1981.6 J/cm^2)

f – 150 J (2123.1 J/cm^2)

e – macrostructure of the repair zone
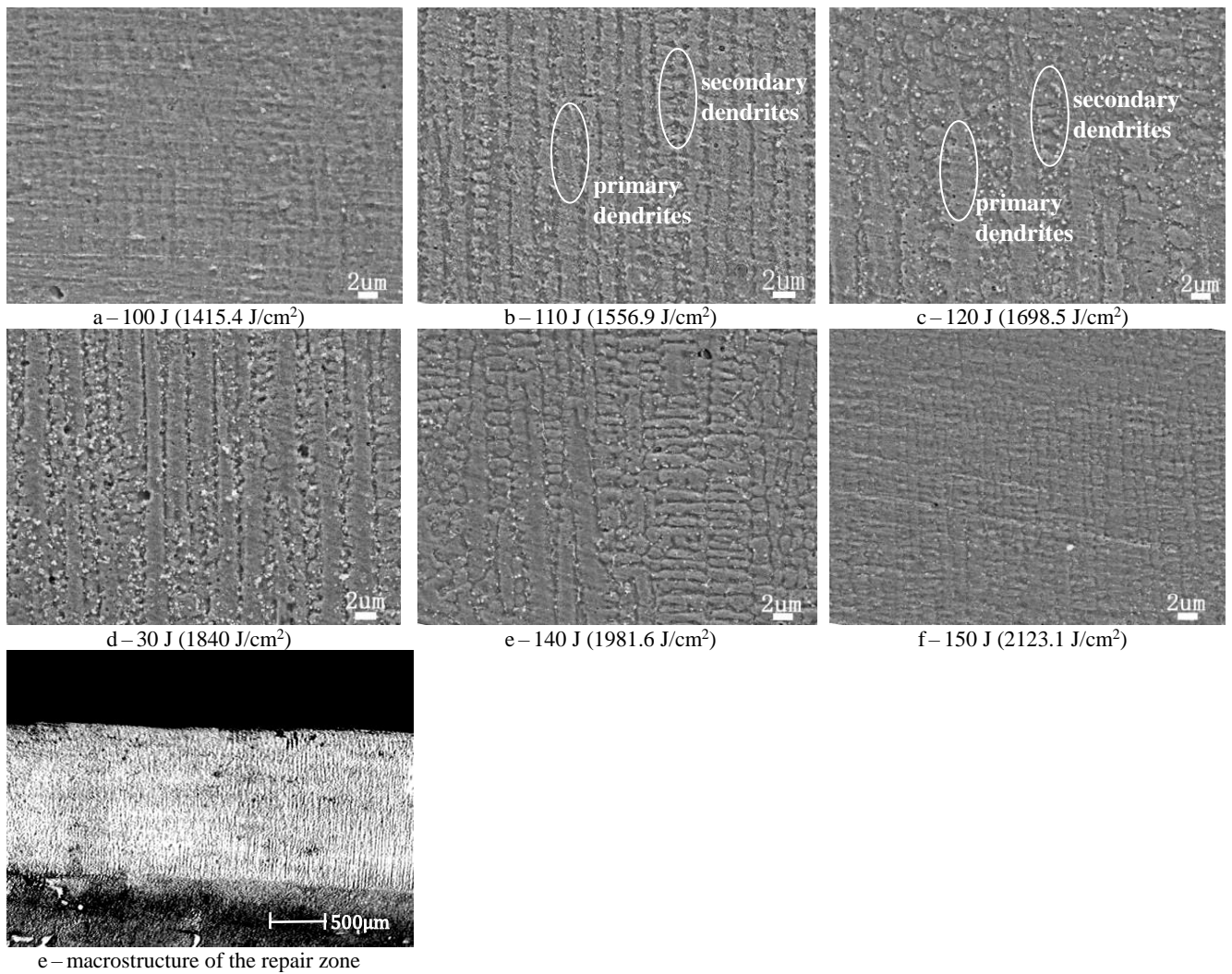
Fig. 1. Appearance of the repair zone for different pulse energy, as observed with the SEM

a – 5 ms

b – 6 ms

c – 7 ms

d – 8 ms

e – 9 ms

f – 10 ms
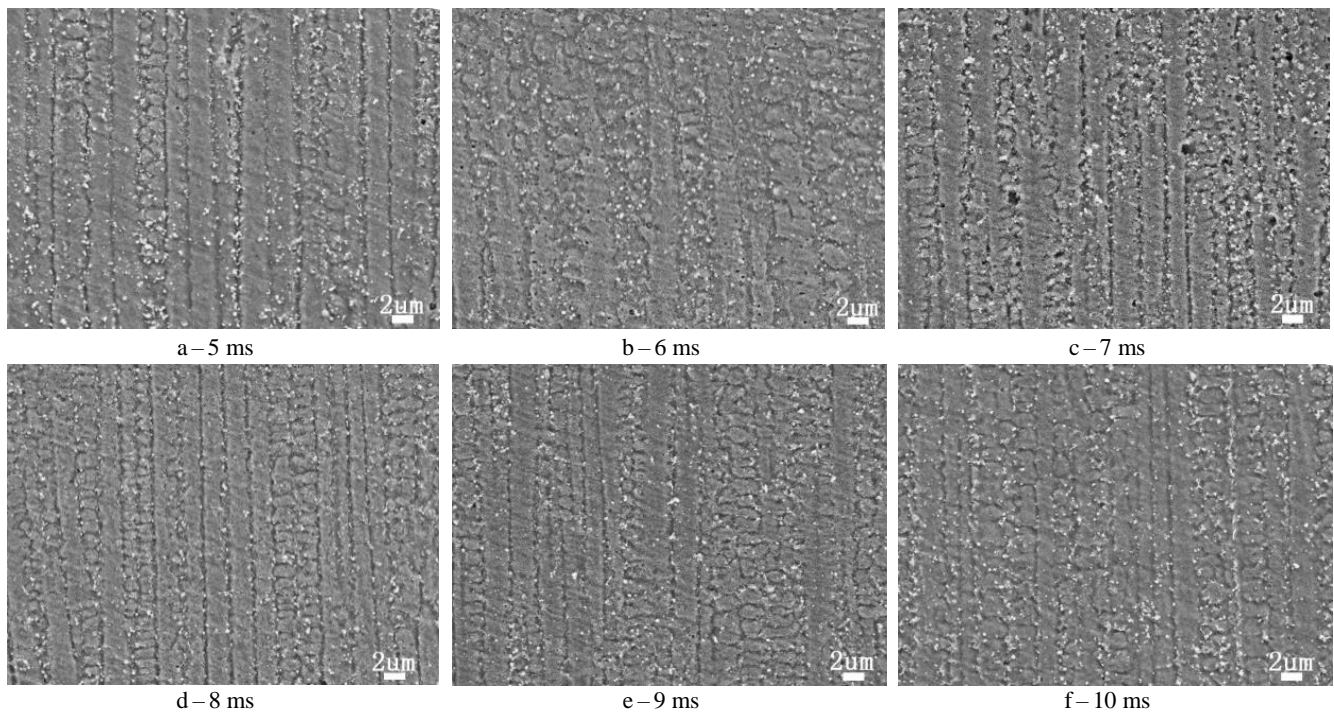
Fig. 2. SEM images of the cladding layer with different pulse-widths, 120 J, 1556.9 J/cm^2
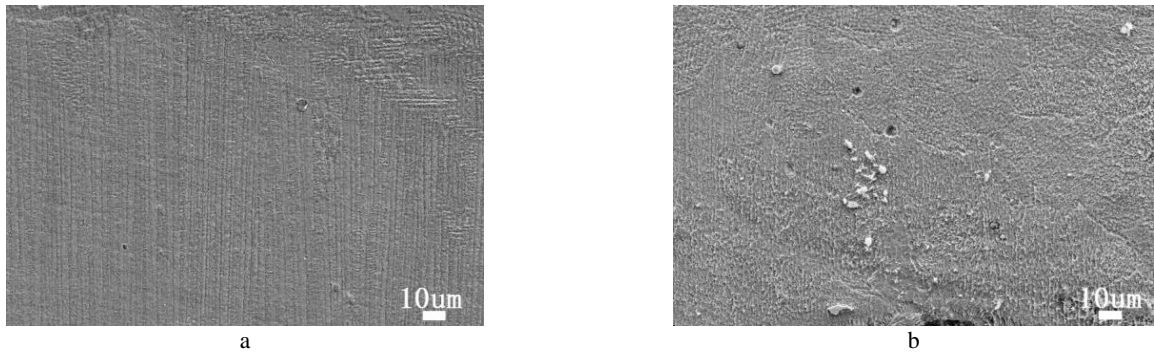
Fig. 3. SEM micrographs of the cladding layer with different scanning speeds: a – 4 mm/s; b – 10 mm/s, 120 J, 1556.9 J/cm^2

3.2. Analysis of element distribution in the repair zone

The distribution of elements in the repair zone is shown in Fig. 4. It is evident that the distribution is quite even. Due to the limited time of the laser fusion process, alloy elements do not diffuse before they solidify. As a result, no macrosegregation is manifested in the repair zone.

The X-ray energy spectrum analysis of the repair zone is presented in Fig. 5. Because of solute convection between the repair zone and the substrate in the cladding process, the substrate is remelted. This changes the components of the repair zone. With the exception of the elements Ni, Co, and Cr, the concentration of all other constituents tends to increase. Oxygen atoms exist in the repair zone, indicating the formation of the oxide of Al_2O_3.
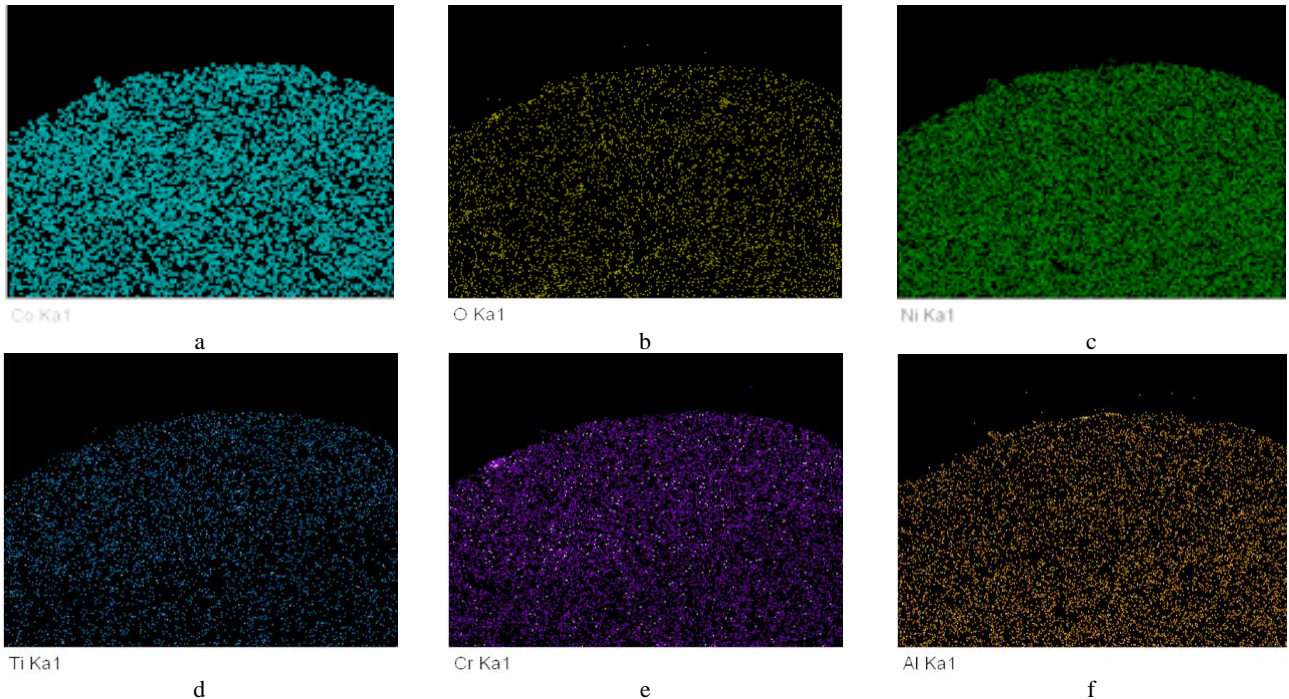

Fig. 4. Constituent element distribution in the repair zone: a – Co; b – O; c – Ni; d – Ti; e – Cr; f – Al
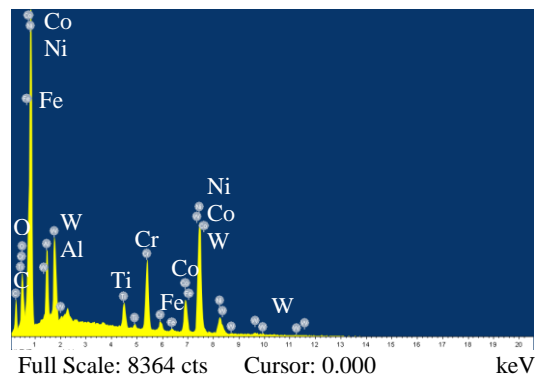

**Fig. 5.** X-ray energy spectrum distribution of the repair zone
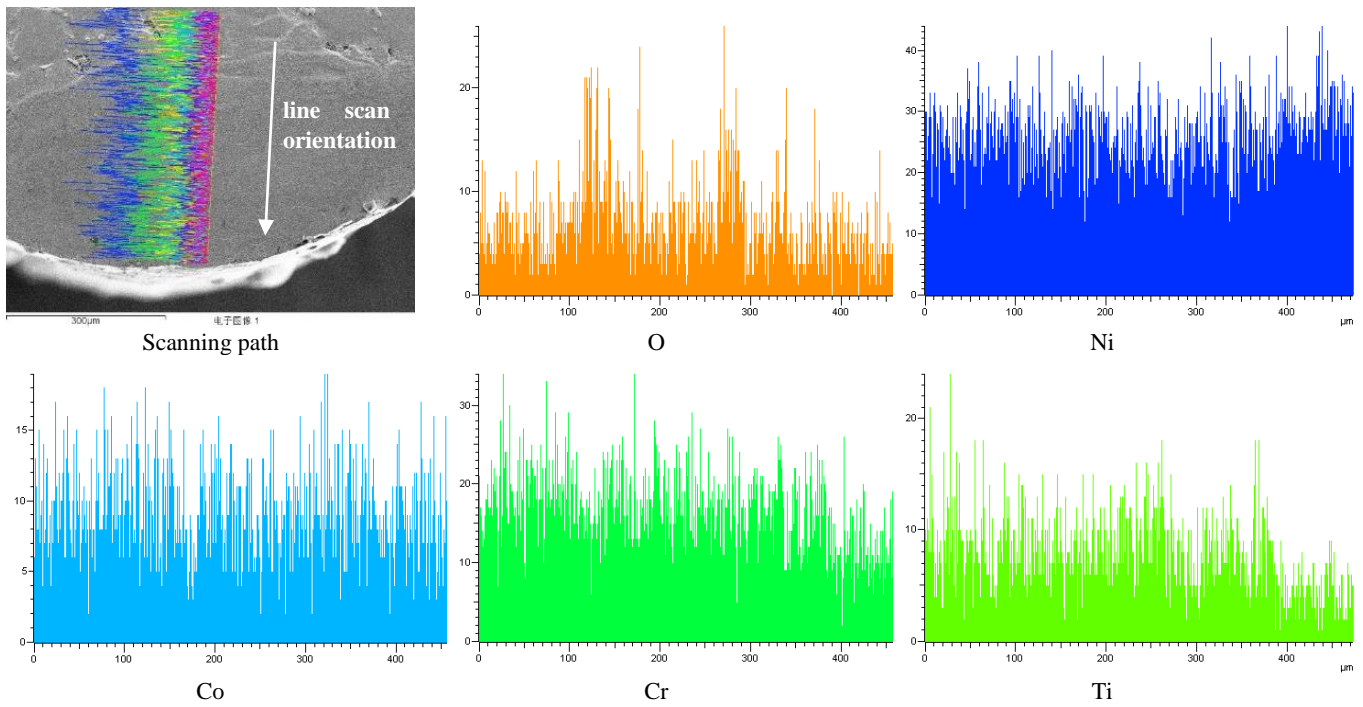
Fig. 6. Line scans for individual alloy constituents

The distribution of the main alloy elements along the vertical direction is shown in Fig. 6. The plots illustrate that there was no obvious variation in the element distribution from the top repair zone to the inner substrate. Alloy distribution in the bonding zone was quite even. The oxygen peak shows up, which is due to the reduced solid solutionization of the aluminum atoms in the mid-repair zone. As a result, more Al_2O_3 molecules are formed from the precipitated aluminum and oxygen, causing the aggregation of oxygen. As tungsten atoms are heavier due to gravity, most are distributed at the bottom of the weld pool.

Macrosegregation in the repair zone is not evident and diffusion of the elements is limited. However, the columnar crystal size is small and microsegregation exists between the centers and the edges of the dendrites, and in between dendrites. The energy spectrum analysis is presented in Fig. 7 and the detailed data are summarized in Table 3.
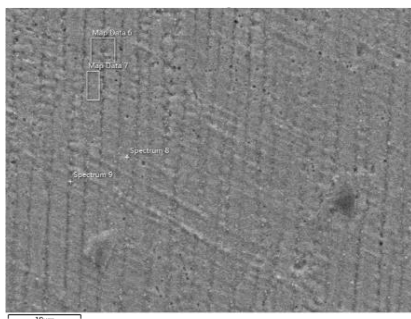

Fig. 7. SEM micrograph of energy spectrum analysis position

It can be seen that Al and Ti are more concentrated in between dendrites than within the dendrites. The reason is as follows: Because the dendrites solidify earlier, elements with lower melting points are more concentrated between the dendrites. That is to say, γ' phase elements such as Al and Ti are concentrated and go through a γ+γ' eutectic reaction. Aluminum and Oxygen atoms that have not melted into the γ' phase form Al_2O_3. The dendrites then are left with almost no oxygen atoms. Elements such as W and Mo are the main ones to form carbides. W atoms solid-solutionize in the molten Ni phase and this increases the wear resistance of the alloy. Tungsten has a high melting point and it will solidify first in the dendrites. Extra molybdenum and carbon atoms combine at the boundary to form carbides. As a result, the Mo concentration is richer between the dendrites than within them.

3.3. Microhardness tests

The microhardness distribution in the repair zone is shown in Fig. 8. The hardness gradient can be observed in the repair zone, the bonding zone, the heat-affected zone, and the substrate. Among these, the repair zone and the bonding zone have significantly higher hardness than the other regions, with an average hardness of 455 HV. This is because the repair zone has a finer structure than the substrate, with a dendrite size about two orders of magnitude smaller than that of the substrate.

Table 3. Element distribution within the repair alloy structure

| Element		C	O	Al	Ti	Cr	Fe	Co	Ni	W	Mo
Mass percentage	In dendrites	0.16	1.04	2.00	2.03	14.5	0.57	17.8	53.8	2.3	5.79
	Between dendrites	6.64	4.78	4.87	5.12	9.3	0.23	16.2	47.3	1.24	7.32
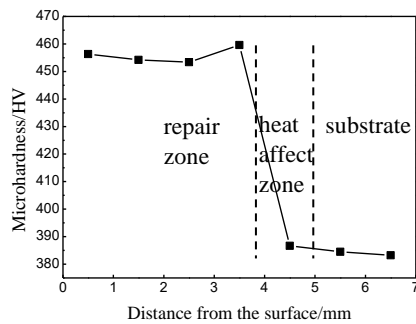
Fig. 8. Microhardness distribution

The repair zone was composed mainly of a very homogeneous base phase γ and precipitated strengthening phase γ'. Due to the large temperature gradient and high solidification rate, the zone is more solid-solutionized than the substrate. In addition, the hardest zone was close to the bonding region and the surface of the repair zone and the part close to the bonding region had a higher hardness than the central zone. This was because tiny isometric crystals are formed at the top of the zone, which imparts a significant strengthening effect on the alloy. In fact, more hard elements, such as W and Mo, are found at the bottom of the repair pool, so the structure is harder in that zone.

3.4. Crack analysis

The orientation of the substrate is different and there is an angle between it and the direction of heat flow. Additionally, the bottom of the molten pool is connected to the well-developed secondary dendrite of the substrate, so the bottom of the repair zone is affected significantly by the orientation of the substrate grains and it is not easy to form a good columnar structure. The number of cracks increase due to the heat input. Some long cracks extend from the substrate to inside the repair area. And some cracks are also present only in the repair area, as shown in Fig. 9.
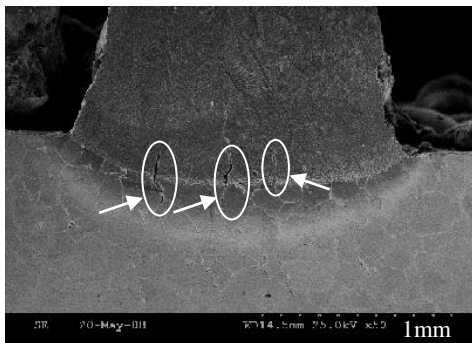

Fig. 9. Cracks inside of the repair zone

Be highly susceptible to heat-induced cracking of the low melting-point eutectic alloys [15], cracks mostly originate from the γ+γ' eutectic. The eutectic, which has a low melting point, is present in the heat-affected zone on the substrate. It does not fully recover when solidification happens, and that leads to the formation of the cracks. The cracks extend themselves along grain boundaries into the repair zone. The repair zone forms γ phase (single-phase nickel-based solid solution) before solidification. It precipitates with γ' phase from the γ phase during the

solidification. At the end of solidification, extra liquid forms eutectic phase γ+γ' at the boundary [16]. Due to the lower reaction temperature of the γ+γ' phase than the solidus temperature, it is likely to form a liquid film at the boundary. This will cause local degradation of the mechanical properties and hence it prompts cracking. The cracks inside the repair zone also happen mostly at the boundary of the repair zone and the substrate. This could be seen from the fact that the dendrites on different sides of the cracks often have different orientations and profiles.

5. CONCLUSIONS

1. It was confirmed that primary dendrite size in the laser repair zone of a simulated turbine blade repair was proportional to the energy and pulse-width, and inversely proportional to the scan speed. After processing, the repair zone was intimately attached to the substrate. The test samples demonstrated co-solidification and continuous columnar crystals were formed with regular alignment. This approach could be used to undertake directional solidification repair of turbine blades.

2. The repair zone did not exhibit significant macrosegregation. A microstructure finer than the substrate was observed. The columnar crystal size was about two orders of magnitude smaller than that of the substrate. Microsegregation was evident between dendrites and between the centers and the edges of dendrites.

3. Microhardness checks showed a descending trend of hardness from the repair zone (455 HV) to the substrate.

REFERENCES

1. **Yan, Y.C., Kang, Y.W., Song, J.X.** Research Progress in Directional Solidification of Nb-Si Based Super Alloy *Materials Review* 28 (1) 2014: pp. 86 – 90. https://doi.org/10.7527/S1000-6893.2014.0138

2. **Guo, H.S., Guo, X.P., Zhao, H.L.** Research Progress in Directional Solidification of Nb-Si Based High Temperature Alloys *Rare Metal Materials and Engineering* 43 (4) 2014: pp. 1019 – 1023.

3. **Han, G.M., Li, F., Sun, B.-D.** Research Progress in Ultrahigh Temperature Nb-Si Based Alloys *Special Casting & Nonferrous Alloys* 38 (10) 2018: pp. 1071 – 1075. https://doi.org/10.15980/j.tzzz.2018.10.008

4. **Ma, D.X., Zhang, Q.Y., Wang, H.Y.** Influence of Process Condition on the Stray Grain Formation in the Single Crystal Blades of Ni-Base Super alloy DD483 *Foundry* 66 (5) 2017: pp. 439 – 444. https://doi.org/10.3969/j.issn.1001-4977.2017.05.001

5. **Pu, K., Qiu, F., Wang, Z.H., Tian, G.L., Zhang, X.D.** Development of Manufacture Technology and Recrystallization Study for Nickel Based Single Crystal Hollow Turbine Blade *Aeronautical Manufacturing Technology*. https://doi.org/10.16080/j.issn1671-833x.2016.21.034

6. **Lu, Y.Z., Xi, H.J., Shen, J., Zheng, W., Xie, G.** Experimental and Simulation Study of Directional Solidification Process for Industrial Gas Turbine Blades Prepared by Liquid Metal Cooling *Acta Metallurgica*

Sinica 5 2015: pp. 603 – 611.
https://doi.org/10.11900/0412.1961.2014.00449

7. **Tang, N., Wang, Y.L., Xu, Q.Y., Zhao, X.H., Liu, B.C.** Numerical Simulation of Directional Solidified Microstructure of Wide-chord Aero Blade by Bridgeman Process *Acta Metallurgica Sinica* 51 (4) 2015: pp. 499 – 512.
https://doi.org/10.11900/0412.1961.2014.00345

8. **Wang, H.B.** Application of Laser Cladding Welding in Repairing Mechanical Parts *Modern Manufacturing Technology and Equipment* 9 2018: pp. 171 – 172.
https://doi.org/10.16107/j.cnki.mmte.2018.0889

9. **Liu, J.W.** Research on Simulation of Directional Solidification Process and Control of Microstructure of Nickel-based Single Crystal Hollow Blades *Jiangsu University* 5 2019: pp. 1 – 20.

10. **Shang, W., Sun, C.B., Liu, Y., Li, B.** Microstructure Simulation to the Solidification Process of Single Crystal Guide Vane *Foundry* 62 (5) 2013: pp. 415 – 419.
https://doi.org/10.3969/j.issn.1001-4977.2013.05.012

11. **Sun, B.C.** Effect of Turbine Blade Casting Process for DZ125 Alloy on Fluorescence Display and Mechanical Properties *Harbin Institute of Technology Master Thesis* 01 2019: pp. 01 – 18.

12. **Chen, M.Y., Wang, H.M., Tian, X.J., Li, J.** Study on Micro-columnar Microstructure of Ni-based Superalloy Fabricated by Laser Melting Deposition *Materials Review* 29 (20) 2015: pp. 101 – 104.
https://doi.org/10.11896/j.issn.1005-023X.2015.20.021

13. **Zhang, D.Y., Li, Z.B., Zhao, H.** Research of the Influence of Processing Parameter on Laser Directional Solidification Structure *Applied Laser* 33 (2) 2013: pp. 113 – 118.
https://doi.org/10.3788/AL20133302.113

14. **Kurz, W., Fisher, D.J.** Dendrite Growth at the Limit of Stability Tip Radius and Spacing *Acta Metall* 29 1981: pp. 11 – 20.
https://doi.org/10.1016/0001-6160(81)90082-1

15. **Sun, H.J., Zhong, M.L., Liu, W.J.** Cracking Sensitivity on Laser Cladding Inconel 738 on Directionally Solidified Ni-base Superalloy *Journal of Aeronautical Materials* 25 (2) 2005: pp. 26 – 31.
https://doi.org/10.3969/j.issn.1005-5053.2005.02.006

16. **Feng, L.P., Lin, X., Chen, D.R.** Influence of The Materials on the Solidification Microstructure of Laser Multi-layer Cladding *Journal of Aeronautical Materials* 24 (1) 2004: pp. 7 – 11.
https://doi.org/10.3969/j.issn.1005-5053.2004.01.002